Transient surface ocean oxygenation recorded in the ~2.66 Ga Jeerinah Formation, Australia

Matthew C. Koehler[1,2*], Roger Buick[1,2], Michael A. Kipp[1,2], Eva E. Stüeken[2,3], and Jonathan Zaloumis[1,4]

[1]Department of Earth & Space Sciences and Astrobiology Program, University of Washington, Seattle WA 98195-1310, USA

[2]Virtual Planetary Laboratory, NASA Astrobiology Institute, Seattle WA 98195-1580, USA

[3]School of Earth and Environmental Sciences, University of St. Andrews, St. Andrews KY16 9AL, Scotland, UK

[4]School of Earth and Space Exploration, Arizona State University, Tempe AZ 85287-1404, USA

**Corresponding Author: koehlerm@uw.edu*

ABSTRACT

Many paleoredox proxies indicate low-level and dynamic incipient oxygenation of Earth's surface environments during the Neoarchean (2.8-2.5 Ga) prior to the Great Oxidation Event (GOE) at ~2.4 Ga. The mode, tempo, and scale of these redox changes are poorly understood because data from various locations and ages suggest both protracted and transient oxygenation. Here we present bulk-rock and kerogen-bound nitrogen isotope ratios as well as bulk-rock selenium abundances and isotope ratios from drill-cores sampled at high stratigraphic resolution through the Jeerinah Formation (~2.66 Ga; Fortescue Group, Western Australia) to test for changes in the redox state of the surface environment. We find that both shallow and deep depositional facies in the Jeerinah Fm display episodes of positive primary $\delta^{15}N$ values ranging from +4 to +6‰, recording aerobic nitrogen cycling that requires free O_2 in the upper water column. Moderate selenium enrichments up to 5.4 ppm in the nearer-shore core may indicate coincident oxidative weathering of sulfide minerals on land, though not to the extent seen in the younger Mt. McRae Shale that records a well-documented 'whiff' of atmospheric oxygen at 2.5 Ga. Unlike the Mt. McRae Shale, Jeerinah selenium isotopes do not show a significant excursion concurrent with the positive $\delta^{15}N$ values. Our data are thus most parsimoniously interpreted as evidence for transient surface ocean oxygenation lasting less than 50 Myr, extending over hundreds of kilometers, and occuring well before the GOE. The nitrogen isotope data clearly record nitrification and denitrification, providing the oldest firm evidence for these microbial metabolisms.

SIGNIFICANCE STATEMENT

Understanding how and when Earth's surface became oxygenated is essential for understanding its biogeochemical evolution. Incipient oxygenation of Earth's surface environments before the Great Oxidation Event (~2.4 Ga; GOE) has been well-documented, but the nature of these redox changes, whether protracted or transient, is poorly understood. We present nitrogen isotope ratios, selenium abundances, and selenium isotope ratios from the Jeerinah Formation (~2.66 Ga; Fortescue Group, Western Australia) that represent (i) high-resolution evidence of transient surface ocean oxygenation ~260 Myr

before the GOE, (ii) a possible muted pulse of oxidative continental weathering, and (iii) the oldest firm evidence for nitrification and denitrification metabolisms. These results, in concert with previous studies, highlight the variability in mechanisms and magnitudes of Neoarchean oxygen fluctuations.

INTRODUCTION

Despite widespread agreement about general trends (1), our understanding of the mode and tempo of Earth's oxygenation still suffers from considerable uncertainties. Among the more salient features of this record is a proposed "whiff" of oxygen in surface environments at 2.5 Ga - well before the onset of the Great Oxidation Event (GOE) at ~2.3-2.4 Ga (2, 3) - which has been identified using combined trace metal and nitrogen isotope datasets collected at high stratigraphic resolution (4–6). Exploration of other Meso- and Neoarchean records has revealed dynamic evolution of surface ocean redox conditions and oxidative continental weathering leading up to the permanent establishment of oxidizing conditions at Earth's surface (7–21). To further elucidate the dynamic redox landscape in the Neoarchean, we conducted a coupled survey of nitrogen and selenium isotopes and abundances at high stratigraphic resolution in two drill cores spanning a near shore-offshore transect across the ~2.66 Ga Jeerinah Formation in Western Australia. These complementary proxies allow us to assess the relative magnitude and spatial extent of redox fluctuations.

Nitrogen is essential for life as we know it and its biogeochemical behavior is highly redox-sensitive. Since at least 3.2 Ga, it is evident that the biosphere has exerted the primary control on Earth's surface nitrogen fluxes, regulating nitrogen availability and speciation in the ocean and atmosphere (22, 23). Metabolisms that drive nitrogen speciation in the ocean (transition of nitrogen among different redox states) can use a variety of electron donors for reduction such as organic matter, Fe^{2+}, and sulfide, but for oxidation are primarily reliant on dissolved O_2 as an electron acceptor due to the high Eh of nitrate (24). Ammonium oxidation to nitrate can occur down to low nM oxygen concentrations (25, 26), which is a fraction of a percent of modern well-oxygenated ocean waters. Thus, a significant pool of nitrate in an ancient ocean would suggest that at least minor amounts of oxygen were freely available to allow for nitrification: the biologically mediated conversion of ammonium to nitrite/nitrate.

Modern microbial metabolisms are known to have a diverse range of effects on the relative abundances of the nitrogen isotopes ^{14}N and ^{15}N (summarized in Table 1 of ref 24, 27, 28). For example, N_2 fixation using Mo-nitrogenase causes an insignificant isotopic fractionation during the conversion of N_2 to organic-bound nitrogen, but biological denitrification of NO_3^- to N_2 strongly prefers ^{14}N, producing isotopically light N_2 gas and an isotopically heavy residual dissolved NO_3^- pool. Hence nitrogen isotopes in ancient sedimentary rocks have allowed paleo-ecological interpretations of nitrogen metabolisms in ancient ecosystems. These interpretations are only semi-quantitative due to overlapping fractionation factors for different metabolic pathways and because of the potential for isotopic resetting by post-depositional alteration. Still, the presence of nitrate in concentrations high enough for significant bio-assimilation can be distinguished isotopically from anaerobic settings that are dominated by nitrogen fixation followed by proximal re-assimilation of liberated ammonium (e.g. 5, 22–24, 29–31).

We also studied the behavior of selenium (Se) – a redox-sensitive element whose oxyanions are stable at similar redox potentials to nitrogen oxyanions – to determine whether changes in marine nitrogen cycling were concurrent with changes in weathering dynamics on land. Unlike nitrate, which is primarily produced during biomass remineralization and nitrification in the water column, Se oxyanions are mainly sourced from oxidative weathering on land (32). Additionally, if Se fluxes are sufficiently large and oxygenated waters sufficiently widespread, Se isotopes can become fractionated during incomplete reduction of Se oxyanions (33). The nitrogen and selenium proxies combined can thus inform us about the loci of oxygenation.

GEOLOGIC SETTING

As part of the Agouron Institute Drilling Project in 2012, two ultra-clean diamond drill cores AIDP-2 and AIDP-3 were sampled across the boundary between the Hamersley and Fortescue Groups in Western Australia. These holes were collared at 21°16'51"S 120°50'02"E (AIDP-2) and 21°46'32"S 117°34'11"E (AIDP-3) across a basinal depth gradient with AIDP-2 intersecting shallower near-shore facies and AIDP-3 deeper offshore facies. AIDP-2 consists of ~158 meters of the Carawine Dolomite that for this study was sampled at low stratigraphic resolution (SI Appendix, Figure S1), and ~128 meters of predominantly black shales from the Jeerinah Formation that were sampled at one-meter resolution. AIDP-3 is ~138 meters deep, capped by the basal Marra Mamba Iron Formation but with samples taken exclusively from the underlying Jeerinah Formation at one-meter resolution. The shallower depositional environment of AIDP-2 is indicated by the stromatolitic carbonates of Carawine Dolomite (34) and by the shoreface setting of the basal Woodiana Member of the Jeerinah Formation which consists of occasionally stromatolitic orthoquartzites (35). In contrast, AIDP-3 transects only a basinal banded iron formation and sulfidic kerogenous shales. The two holes can be stratigraphically correlated using a horizon of meteorite impact spherules (36), which occurs in a ~20 meter thick megabreccia towards the bottom of the Carawine Dolomite in AIDP-2 and in a 1 centimeter thick graded spherule layer in the upper Jeerinah Formation in AIDP-3 (SI Appendix, Figure S2). Rocks from both AIDP-2 and AIDP-3 are generally thought to be within the prehnite-pumpellyite metamorphic facies (37) but an alternative upper greenschist facies interpretation exists (38). However, this latter interpretation is inconsistent with the pelitic mineralogy of the AIDP shales as key index minerals of upper greenschist conditions (e.g. biotite, chloritoid) are absent. Also, it depends upon a chlorite geothermometer (39) that (i) unjustifiably assumes all iron in the chlorite is Fe^{2+}, which can lead to temperature overestimations (40), and (ii) yields infeasibly broad temperature ranges (>140°C) for samples in close stratigraphic proximity. Hence we favor the prehnite-pumpellyite metamorphic facies assignment (addressed further in the SI Appendix).

METHODS

Sample preparation and analytical procedures for bulk rock analyses of nitrogen isotopes followed the methodology outlined in (31, 41) and Se abundances and isotopes were determined using the protocol described in (42); for details see the SI Appendix. The linear regression model used to identify the stratigraphic location of significant shifts in

$\delta^{15}N_{bulk}$ followed the methodology reported in (43), and is described in greater detail in the SI Appendix.

RESULTS

Se abundances are tightly scattered around an average of 1.2 ± 1.1 ppm throughout both cores but a moderate excursion up to 5.4 ppm occurs around 363 m in AIDP-2. After normalizing the data to Al, total organic carbon (TOC), and total sulfur (TS), the Se excursion in AIDP-2 still appears statistically significant (Figures 1B,C,D, and SI Appendix, Figures S3 and S4). Multiple regression confirms this inference, showing that less than half of the observed Se enrichment can be explained by lithological variability (R^2 = 0.49; Figure 1B,C,D). $\delta^{82/78}$Se shows no systematic trend across either of the two cores (average +0.3 ± 0.3 ‰). In contrast, δ^{15}N displays a large range from -2‰ to +14‰ with systematic shifts detected by our linear regression model. This identified three distinct stages (I to III from oldest to youngest) in each core (Table 1). The only exception to the model boundary placement is the boundary between stage *I* and *II* in AIDP-3, where the boundary position was handpicked based on marked changes in TOC [%], TN [%], and C/N ratios [atomic]. Importantly, this boundary still falls within the range of stratigraphic positions where the model predicts a significant change in $\delta^{15}N_{bulk}$ values.

AIDP-2: Stage *I* in AIDP-2 is characterized by the most variable $\delta^{15}N_{bulk}$ values in the core, averaging around +2.8‰. In this stage TOC [%] and TN [%] are at their lowest. From stage *I* to stage *II* $\delta^{15}N_{bulk}$ suddenly increase by an average of ~1.5‰ to the highest values recorded in the core (+5.43‰) and become less variable. This rise in $\delta^{15}N_{bulk}$ values is associated with increases in both TOC [%] and TN [%] by about a factor of 3. From stage *II* to stage *III* $\delta^{15}N_{bulk}$ values decrease by 4‰ on average to a minimum of -0.71‰. TOC [%] and TN [%] also decrease across this transition, but not to levels as low as in stage *I*. $\delta^{15}N_{kerogen}$ values are systematically lower than $\delta^{15}N_{bulk}$ measurements throughout the core by an average of 1.6‰ ± 0.9‰, and so show the same general trend as $\delta^{15}N_{bulk}$ values across all three stages (Figure 2).

AIDP-3: Stage *I* in AIDP-3 has the most positive and variable $\delta^{15}N_{bulk}$ values and C/N [atomic] ratios in either core, averaging +11.0‰ and 174 respectively. Notably, in this same stage, TOC [%] and TN [%] averages are the lowest in either core. Across the boundary between stages *I* and *II*, $\delta^{15}N_{bulk}$ values decrease by 5‰ on average (Figure 3). TOC [%] and TN [%] values both increase by over a factor of 3, and C/N [atomic] ratios decrease to an average similar to all stages apart from stage *I* of AIDP-3. The transition from stage *II* to stage *III* is defined by another decrease in $\delta^{15}N_{bulk}$ of about 4‰ on average, similar to the stage *II-III* transition in AIDP-2. TOC [%], TN [%], and C/N ratios [atomic] do not change significantly from stage *II* to stage *III*.

Like AIDP-2, in AIDP-3 $\delta^{15}N_{kerogen}$ values are systematically lower than $\delta^{15}N_{bulk}$. Whereas the average difference between the two measurements is consistent throughout AIDP-2, in AIDP-3 it varies in a stepwise fashion throughout the core; the smallest differences are in stage *III* and the largest are in stage *I*. A noteworthy relationship in stage *I* is that $\delta^{15}N_{kerogen}$ values correlate strongly with atomic $C/N_{kerogen}$ and C/N_{bulk} ratios (Figure 1A). This is not the case in stages *II* and *III*, and all of AIDP-2.

DISCUSSION

Proxy alteration: Post-depositional processes such as diagenesis and metamorphism have the potential to alter the primary nitrogen and Se isotopic signals preserved in sedimentary rocks. For example, Se isotope fractionation could potentially occur during diagenetic oxyanion reduction. However, this would require the presence of a stable Se oxyanion reservoir in the overlying water column, which would in turn imply oxic conditions. Such diagenetic Se reactions would therefore strengthen environmental redox signals. During metamorphism, Se is fairly immobile (44), and so its isotopic ratios are unlikely to be altered. Nitrogen isotopes, on the other hand, can undergo more significant alteration during diagenesis and metamorphism (45). The $\delta^{15}N$ of sinking and sediment biomass can increase during early diagenesis under oxic conditions through the preferential remineralization, oxidation, and loss of ^{14}N (common in modern marine settings), but is less susceptible to alteration under the mainly anoxic bottom waters/sediments (46–48) characteristic of the Neoarchean. It is possible that for samples with initially positive $\delta^{15}N_{bulk}$ values, early diagenesis under anoxic conditions can decrease $\delta^{15}N_{bulk}$ values by the addition of isotopically light ($\delta^{15}N$ of -2‰ to +1‰) biomass via the in-situ growth of nitrogen-fixing bacteria; samples that have a primary $\delta^{15}N_{bulk}$ signal around 0‰ would not be significantly affected by this mechanism (49–51). Primary $\delta^{15}N$ values may also decrease by the preferential deamination of ^{15}N-enriched organic compounds such as proteins (49). Even if more relevant in the Neoarchean, neither of these mechanisms can fully account for the shifts in $\delta^{15}N_{bulk}$ values of up to 4‰ between stages in both cores, nor would they affect our interpretations regarding episodes of enriched $\delta^{15}N$ values.

Anoxic diagenesis may lead to small isotopic differences between the kerogen and silicate nitrogen fractions and even smaller isotopic changes in bulk rock measurements, but metamorphism/metasomatism can lead to greater isotopic disparity and changes that are not always predictable (e.g. 52, 53). Below greenschist facies, such thermal effects can lead to changes in the primary nitrogen isotopic signal of bulk rocks by 1-2‰ (45). As previously mentioned, the Carawine Dolomite and Jeerinah Formation were likely metamorphosed to prehnite-pumpellyite grade (37), and so may have been subject to these small changes to the primary $\delta^{15}N$ values. As metamorphic grade and metasomatic alteration increases, so does the difference in $\delta^{15}N$ between bulk rock and kerogen fractions, which may reach up to 13‰ (54).

To test if metamorphism/metasomatism has affected our samples, we considered the relationship between $\delta^{15}N$ values and C/N ratios, as well as the difference in $\delta^{15}N$ values between the two nitrogen fractions (kerogen and silicate). If thermal processes have significantly affected our samples, increasing $\delta^{15}N$ values should correspond to increasing C/N ratios as nitrogen is more mobile than carbon and ^{14}N is more mobile than ^{15}N under such conditions. The only samples that show this relationship come from stage 1 in AIDP-3 (Figure 1A). This is also the stage where the differences in $\delta^{15}N$ values between the two nitrogen fractions are the greatest and most variable. Because of this, stage 1 of AIDP-3 evidently displays a secondary isotopic signal due to thermal alteration. This most likely had a metasomatic component, as the kerogen samples are not persistently more altered (higher C/N and $\delta^{15}N$) with stratigraphic depth but show local variability that could have resulted from focused fluid-rock interactions. This is consistent with previous observations that

underlying basalt units locally experienced metasomatic alteration (55). Indeed, the basalt underlying the Jeerinah Fm in AIDP-3 has metamorphic/metasomatic textures including zones of K-feldspar spherulites, veins and amygdales filled with chlorite, calcite, silica, and patches of sericitization, all indicating multiple periods of metasomatic alteration (SI Appendix, Figure S5a-h). Because all samples from AIDP-2 and from stages II and III of AIDP-3 lack petrographic and geochemical signs of significant thermal alteration, the $\delta^{15}N$ values from these stages are interpreted to be close to primary compositions.

Interpretation of nitrogen isotopic data: $\delta^{15}N$ values between -2‰ and +1‰, as seen in AIDP-2 Stage III, are generally interpreted to reflect marine nitrogen cycling dominated by nitrogen fixation using Mo-nitrogenase (56). Elevated $\delta^{15}N$ values >+1‰, as in all other stages, can be interpreted in one of three ways (e.g. 30, 31; SI Appendix, Figure S6): (i) Partial bio-assimilation from a dissolved NH_4^+ pool that would preferentially remove ^{14}N, locally creating isotopically light biomass and an isotopically heavy residual NH_4^+ pool. If this heavy residual pool were transported to another location in the basin, it could be fully assimilated and biomass there would record isotopically heavy $\delta^{15}N$ values (57). However, because AIDP-2 (shallow) and AIDP-3 (deep) represent a broad cross-basinal transect and no corresponding isotopically light values (<-2‰) were encountered anywhere, there is no evidence to suggest that this process was responsible for the heavy $\delta^{15}N$ values in either core. (ii) Partial nitrification of an ammonium pool that preferentially selected ^{14}N followed by quantitative denitrification of the resulting nitrate would leave the residual ammonium isotopically heavy. Bio-assimilation from this ammonium pool would result in isotopically heavy biomass (58). (iii) Quantitative nitrification of an ammonium pool followed by partial denitrification of the resulting nitrate pool that preferentially removed ^{14}N would leave residual nitrate isotopically enriched in ^{15}N (5, 29). Assimilation of this heavy nitrate pool would yield $\delta^{15}N$-enriched biomass. This mechanism is largely responsible for the enriched $\delta^{15}N$ values of nitrate in the modern deep ocean that are spatially heterogeneous (ranging from +2‰ to +20‰) but show an average around +5‰ (59). The lack of very light $\delta^{15}N$ values suggests that mechanisms (ii) or (iii), both requiring free O_2 for nitrification, best explain our data. Mechanism (ii) should yield highly variable $\delta^{15}N$ values because it lacks an isotopically heavy nitrogen sink from the ocean (31), but such variability is not seen in most of the AIDP stages. We thus propose that mechanism (iii) probably prevailed. In either case, the isotopically enriched nitrogen data require oxic conditions in marine surface waters.

Interpretation of selenium concentrations and isotopic ratios: The extent of oxygenation can be further elucidated using Se isotopes and abundances. The peak in Se abundances during Stage II of the AIDP-2 core may reflect (i) enhanced oxidative terrestrial weathering, or (ii) enhanced delivery of volcanically derived SeO_2. We cannot definitively rule out a volcanic Se source for the Se enrichment in AIDP-2, as the volcanic flux of Se to marine environments may have been comparable to, or greater than, the Se flux from oxidative weathering under low O_2 conditions (32). We would, however, expect that such an event should have been more uniformly distributed across the basin and recorded in AIDP-3. As AIDP-3 does not show any significant Se enrichment, our data are perhaps more consistent with a small fluvial Se influx that was sequestered near-shore under dominantly anoxic bottom waters. In any case, the <6 ppm Se enrichment is noticeably smaller than that during the 2.50 Ga whiff of oxygen recorded in the Mt McRae Shale (6), where Se abundances

reach 20 ppm. This difference suggests that the Se flux to the ocean was considerably less during the Jeerinah oxygenation event. This conclusion is further supported by the Jeerinah Se isotopic data which nearly all fall within the crustal range (-0.3 to +0.6‰; ref 60) indicating that any Se oxyanion reservoir was small and nearly quantitatively sequestered in near-shore environments, unlike the Mt McRae Shale which shows a marked positive excursion in $\delta^{82/78}$Se to +1.4‰ (6). So, while the nitrogen data are comparable between the two events, the Se data suggest that the magnitude of oxidative weathering was smaller at 2.66 Ga than at 2.50 Ga.

Transient surface ocean oxygenation in the Neoarchean: mode and tempo: A transient enrichment in Archean sedimentary δ^{15}N at 2.5 Ga has previously been linked to an oxygen "whiff" before the GOE (5), and this AIDP dataset extends such evidence for surface ocean oxygenation back by ~160 Ma. Godfrey & Falkowski (29) previously reported several elevated δ^{15}N measurements from a roughly coeval section in the Transvaal Supergroup in South Africa sampled at coarse stratigraphic resolution, which are also consistent with aerobic nitrogen cycling in the surface ocean. However, the δ^{15}N data presented here show that surface ocean oxygenation was a transient phenomenon lasting 50 Myr or less (see text below for calculations). It also provides direct evidence that this episode of late Archean oxygenation extended over hundreds of kilometers, with surface waters evidently holding nM to μM concentrations of dissolved O_2 allowing widespread nitrification (25, 26), as previously predicted (61).

The mode of oxygenation cannot be resolved using nitrogen isotopes alone. Aerobic nitrogen cycling requires bioavailable trace metals such as Mo, Cu, and Fe along with free O_2 and dissolved NH_4^+, and it is not clear which was limiting before and after stage II. Surface ocean oxygenation could have been a purely oceanographic event driven by changes in upwelling that delivered nutrients like Fe and NH_4^+ to the photic zone stimulating cyanobacterial productivity (61). Alternatively, mild oxidative weathering on land during stage II could have supplied bioessential trace metals to basin surface waters without supplying much Se, due to its high Eh. This could have resulted from localized oxidative weathering beneath non-marine cyanobacterial mats, hypothesized to have been significant before the GOE (62), or from a small global pulse in atmospheric oxygen levels. If cyanobacteria and nitrifiers were trace metal limited (63, 64), either mechanism would spur regional oxygen production allowing free O_2 and NO_3^- to accumulate in the photic zone. Both are consistent with the positive δ^{15}N values in stage *II* of the two cores, as well as the observed Se enrichment in AIDP-2.

If the Se enrichment in AIDP-2 were due to weak oxidative weathering of continental material (our preferred interpretation) then oxygenation of the surface ocean and mobilization of Se oxyanions were out of phase, as indicated by the δ^{15}N and [Se] values. Regardless of whether surface ocean oxygenation resulted from delivery of nutrients by upwelling or oxidative weathering, the Se peak could indicate a period of more vigorous oxidative continental weathering, but not to the extent of the 2.5 Ga Mt McRae "whiff". The occurrence of similarly positive nitrogen isotope values in rocks of similar age from South Africa indicates that surface oceanic oxygenation leading to aerobic nitrogen cycling (29) may have been relatively widespread at this time. Fluctuating balances between atmospheric O_2 sources and sinks could have led to transient increases in atmospheric O_2 of various magnitudes, consistent with a more global positive δ^{15}N signal and the Se enrichment.

Alternatively, terrestrial cyanobacterial mat proliferation under a transient organic haze (18, 65, 66) providing temporary UV protection (67) may have increased the oxidative weathering flux of Se, but the feedback between O_2 generation, aerobic methane oxidation, and haze formation needs to be explored in greater detail.

As mass independent fractionation of sulfur isotopes is persistent throughout the Jeerinah Fm (68, 69), any atmospheric oxygenation event could have only been of limited magnitude. The duration of the $\delta^{15}N$ excursion in AIDP-2, covering ~35 meters of shale deposition, suggests that the shifting balance between O_2 sources and sinks driving oxygenation would have operated on a geologically rapid (< 50 Myr) timescale[1]. As the Se abundance excursion is even more stratigraphically restricted (<20 meters), any interval of atmospheric oxygenation would have been proportionately shorter.

The $\delta^{15}N$ data also clearly indicate that the microbial metabolisms of nitrification and denitrification had already evolved by ~2.66 Ga (SI Appendix, Figure S7), confirming the few data points previously reported from similarly ancient rocks from South Africa (29). Both nitrification and denitrification are complex pathways involving many redox steps utilizing multiple metalloenzymes, which on the modern Earth are typically mediated by microbial consortia or, in rare cases, by individual microbial taxa (72, 73). This implies that, by the mid-Neoarchean, microbes had developed either evolutionary or ecological sophistication comparable to their modern counterparts.

CONCLUSION

The data presented here record a second Archean event characterized by transient oxygenation of the surface ocean. While the nitrogen isotopic signal is similar in magnitude to the 2.50 Ga Mt. McRae "whiff" of oxygen, the Jeerinah event shows a smaller selenium enrichment and no isotopic excursion in $\delta^{82/78}Se$, suggesting that terrestrial oxidative weathering was weaker during this earlier episode. When viewed at high resolution, these data show that oxygenated surface waters both preceded and post-dated the oxidative weathering signal of selenium, perhaps indicating that local production of oxygen eventually enabled more vigorous sulfide dissolution on land. These results highlight the variability in mechanisms and magnitudes of Neoarchean oxygen fluctuations and demonstrate the importance of feedbacks between biogenic oxygen production, oxidative weathering, and nutrient fluxes during the prelude to the permanent oxygenation of Earth's surface environment.

Acknowledgements

We thank the Agouron Institute, John Abelson and Melvin Simon for funding the drilling of AIDP-2 and AIDP-3, NASA grant NNX16AI37G and NSF FESD grant 338810 to R.B. for funding the analyses, NSF Graduate Research Fellowship funding to M.A.K. and J.Z., and

[1] The top and bottom of the Jeerinah Formation are dated to 2.629±5 (70) and 2.684±6 (71) respectively (differences of 44 Ma minimum and 66 Ma maximum). The positive $\delta^{15}N$ values in stage II occur in ~30m of black shale in the middle of the Jeerinah in both cores, accounting for < 25% of the formation's total thickness. It is therefore likely that oxygenation occurred on a timescale perhaps much less than 50 Ma, assuming similar deposition rates between the two sections.

U.W. ESS Departmental Awards to M.C.K. for other support. We thank the U.W. Isolab, the U.W. non-traditional isotope laboratory, Andy Schauer, Scott Kuehner, Bruce Nelson, and Fang-Zhen Teng for technical support. We also thank Chad Ostrander, Mou Roy, and the Anbar lab at ASU for the aluminum data, as well as Iadviga Zhelezinskaia and Jay Kaufman for the sulfur data.

REFERENCES

1. Lyons TW, Reinhard CT, Planavsky NJ (2014) The rise of oxygen in Earth's early ocean and atmosphere. *Nature* 506(7488):307–315.
2. Bekker A, et al. (2004) Dating the rise of atmospheric oxygen. *Nature* 427(6970):117–120.
3. Gumsley AP, et al. (2017) Timing and tempo of the Great Oxidation Event. *Proc Natl Acad Sci U S A* 114(8):1811–1816.
4. Anbar AD, et al. (2007) A Whiff of Oxygen Before the Great Oxidation Event? *Science* 317(5846):1903–1906.
5. Garvin J, Buick R, Anbar AD, Arnold GL, Kaufman AJ (2009) Isotopic Evidence for an Aerobic Nitrogen Cycle in the Latest Archean. *Science* 323(5917):1045–1048.
6. Stueeken EE, Buick R, Anbar AD (2015) Selenium isotopes support free O-2 in the latest Archean. *Geology* 43(3):259–262.
7. Crowe SA, et al. (2013) Atmospheric oxygenation three billion years ago. *Nature* 501(7468):535–538.
8. Eigenbrode JL, Freeman KH (2006) Late Archean rise of aerobic microbial ecosystems. *Proc Natl Acad Sci* 103(43):15759–15764.
9. Gregory DD, et al. (2015) The chemical conditions of the late Archean Hamersley basin inferred from whole rock and pyrite geochemistry with Delta S-33 and delta S-34 isotope analyses. *Geochim Cosmochim Acta* 149:223–250.
10. Kendall B, Creaser RA, Reinhard CT, Lyons TW, Anbar AD (2015) Transient episodes of mild environmental oxygenation and oxidative continental weathering during the late Archean. *Sci Adv* 1(10):e1500777.
11. Kendall B, et al. (2010) Pervasive oxygenation along late Archaean ocean margins. *Nat Geosci* 3(9):647–652.
12. Kurzweil F, Wille M, Schoenberg R, Taubald H, Van Kranendonk MJ (2015) Continuously increasing δ98Mo values in Neoarchean black shales and iron formations from the Hamersley Basin. *Geochim Cosmochim Acta* 164:523–542.
13. Kurzweil F, et al. (2013) Atmospheric sulfur rearrangement 2.7 billion years ago: Evidence for oxygenic photosynthesis. *Earth Planet Sci Lett* 366:17–26.
14. Planavsky NJ, et al. (2014) Evidence for oxygenic photosynthesis half a billion years before the Great Oxidation Event. *Nat Geosci* 7(4):283–286.
15. Siebert C, Kramers JD, Meisel T, Morel P, Nagler TF (2005) PGE, Re-Os, and Mo isotope systematics in Archean and early Proterozoic sedimentary systems as proxies for redox conditions of the early Earth. *Geochim Cosmochim Acta* 69(7):1787–1801.
16. Stüeken EE, Catling DC, Buick R (2012) Contributions to late Archaean sulphur cycling by life on land. *Nat Geosci* 5(10):722–725.

17. Wille M, et al. (2007) Evidence for a gradual rise of oxygen between 2.6 and 2.5Ga from Mo isotopes and Re-PGE signatures in shales. *Geochim Cosmochim Acta* 71(10):2417–2435.
18. Zerkle AL, Claire M, Domagal-Goldman SD, Farquhar J, Poulton SW (2012) A bistable organic-rich atmosphere on the Neoarchaean Earth. *Nat Geosci* 5(5):359–363.
19. Eickmann B, et al. (2018) Isotopic evidence for oxygenated Mesoarchaean shallow oceans. *Nat Geosci*:11: 133-138.
20. Homann M, Heubeck C, Airo A, Tice MM (2015) Morphological adaptations of 3.22 Ga-old tufted microbial mats to Archean coastal habitats (Moodies Group, Barberton Greenstone Belt, South Africa). *Precambrian Res* 266:47–64.
21. Riding R, Fralick P, Liang L (2014) Identification of an Archean marine oxygen oasis. *Precambrian Res* 251:232–237.
22. Ader M, et al. (2016) Interpretation of the nitrogen isotopic composition of Precambrian sedimentary rocks: Assumptions and perspectives. *Chem Geol* 429:93–110.
23. Stueeken EE, Buick R, Guy BM, Koehler MC (2015) Isotopic evidence for biological nitrogen fixation by molybdenum-nitrogenase from 3.2 Gyr. *Nature* 520(7549):666-U178.
24. Stüeken EE, Kipp MA, Koehler MC, Buick R (2016) The evolution of Earth's biogeochemical nitrogen cycle. *Earth-Sci Rev* 160:220–239.
25. Bristow LA, et al. (2016) Ammonium and nitrite oxidation at nanomolar oxygen concentrations in oxygen minimum zone waters. *Proc Natl Acad Sci U S A* 113(38):10601–10606.
26. Bristow LA, et al. (2017) N-2 production rates limited by nitrite availability in the Bay of Bengal oxygen minimum zone. *Nat Geosci* 10(1):24–29.
27. Casciotti KL (2009) Inverse kinetic isotope fractionation during bacterial nitrite oxidation. *Geochim Cosmochim Acta* 73(7):2061–2076.
28. Robinson D (2001) δ15N as an integrator of the nitrogen cycle. *Trends Ecol Evol* 16(3):153–162.
29. Godfrey LV, Falkowski PG (2009) The cycling and redox state of nitrogen in the Archaean ocean. *Nat Geosci* 2(10):725–729.
30. Koehler MC, Stueeken EE, Kipp MA, Buick R, Knoll AH (2017) Spatial and temporal trends in Precambrian nitrogen cycling: A Mesoproterozoic offshore nitrate minimum. *Geochim Cosmochim Acta* 198:315–337.
31. Stueeken EE (2013) A test of the nitrogen-limitation hypothesis for retarded eukaryote radiation: Nitrogen isotopes across a Mesoproterozoic basinal profile. *Geochim Cosmochim Acta* 120:121–139.
32. Stueeken EE, et al. (2015) The evolution of the global selenium cycle: Secular trends in Se isotopes and abundances. *Geochim Cosmochim Acta* 162:109–125.
33. Johnson TM, Herbel MJ, Bullen TD, Zawislanski PT (1999) Selenium isotope ratios as indicators of selenium sources and oxyanion reduction. *Geochim Cosmochim Acta* 63(18):2775–2783.
34. Murphy MA, Sumner DY (2008) Tube structures of probable microbial origin in the Neoarchean Carawine Dolomite, Hamersley Basin, Western Australia. *Geobiology* 6(1):83–93.
35. Nishizawa M, et al. (2010) Grain-scale iron isotopic distribution of pyrite from Precambrian shallow marine carbonate revealed by a femtosecond laser ablation

multicollector ICP-MS technique: Possible proxy for the redox state of ancient seawater. *Geochim Cosmochim Acta* 74(9):2760–2778.
36. Rasmussen B, Blake TS, Fletcher IR (2005) U-Pb zircon age constraints on the Hamersley spherule beds: Evidence for a single 2.63 Ga Jeerinah-Carawine impact ejecta layer. *Geology* 33(9):725–728.
37. French KL, et al. (2015) Reappraisal of hydrocarbon biomarkers in Archean rocks. *Proc Natl Acad Sci U S A* 112(19):5915–5920.
38. Peters CA, Piazolo S, Webb GE, Dutkiewicz A, George SC (2016) In search of early life: Carbonate veins in Archean metamorphic rocks as potential hosts of biomarkers. *Earth Planet Sci Lett* 453:44–55.
39. Lanari P, Wagner T, Vidal O (2014) A thermodynamic model for di-trioctahedral chlorite from experimental and natural data in the system MgO–FeO–Al 2 O 3–SiO 2–H 2 O: applications to P–T sections and geothermometry. *Contrib Mineral Petrol* 167(2):968.
40. Vidal O, Lanari P, Munoz M, Bourdelle F, De Andrade V (2016) Deciphering temperature, pressure and oxygen-activity conditions of chlorite formation. *Clay Miner* 51(4):615–633.
41. Robl TL, Davis BH (1993) Comparison of the HF-HCl and HF-BF3 maceration techniques and the chemistry of resultant organic concentrates. *Org Geochem* 20(2):249–255.
42. Stüeken EE, Foriel J, Nelson BK, Buick R, Catling DC (2013) Selenium isotope analysis of organic-rich shales: advances in sample preparation and isobaric interference correction. *J Anal At Spectrom* 28(11):1734–1749.
43. WAIS Divide Project Members, et al. (2013) Onset of deglacial warming in West Antarctica driven by local orbital forcing. *Nature* 500(7463):440–444.
44. Large RR, et al. (2014) Trace element content of sedimentary pyrite as a new proxy for deep-time ocean-atmosphere evolution. *Earth Planet Sci Lett* 389:209–220.
45. Stueken EE, Zaloumis J, Meixnerova J, Buick R (2017) Differential metamorphic effects on nitrogen isotopes in kerogen extracts and bulk rocks. *Geochim Cosmochim Acta* 217:80–94.
46. Altabet Mark A., Francois Roger (2012) Sedimentary nitrogen isotopic ratio as a recorder for surface ocean nitrate utilization. *Glob Biogeochem Cycles* 8(1):103–116.
47. Thunell Robert C., Sigman Daniel M., Muller-Karger Frank, Astor Yrene, Varela Ramon (2004) Nitrogen isotope dynamics of the Cariaco Basin, Venezuela. *Glob Biogeochem Cycles* 18(3). doi:10.1029/2003GB002185.
48. Möbius J (2013) Isotope fractionation during nitrogen remineralization (ammonification): Implications for nitrogen isotope biogeochemistry. *Geochim Cosmochim Acta* 105:422–432.
49. Lehmann MF, Bernasconi SM, Barbieri A, McKenzie JA (2002) Preservation of organic matter and alteration of its carbon and nitrogen isotope composition during simulated and in situ early sedimentary diagenesis. *Geochim Cosmochim Acta* 66(20):3573–3584.
50. Fry B, et al. (1991) Stable Isotope Studies of the Carbon, Nitrogen and Sulfur Cycles in the Black-Sea and the Cariaco Trench. *Deep-Sea Res Part -Oceanogr Res Pap* 38:S1003–S1019.
51. Libes S, Deuser W (1988) The Isotope Geochemistry of Particulate Nitrogen in the Peru Upwelling Area and the Gulf of Maine. *Deep-Sea Res Part -Oceanogr Res Pap* 35(4):517–533.

52. Haendel D, Muhle K, Nitzsche H, Stiehl G, Wand U (1986) Isotopic Variations of the Fixed Nitrogen in Metamorphic Rocks. *Geochim Cosmochim Acta* 50(5):749–758.
53. Jia Y (2006) Nitrogen isotope fractionations during progressive metamorphism: A case study from the Paleozoic Cooma metasedimentary complex, southeastern Australia. *Geochim Cosmochim Acta* 70(20):5201–5214.
54. Godfrey LV, Poulton SW, Bebout GE, Fralick PW (2013) Stability of the nitrogen cycle during development of sulfidic water in the redox-stratified late Paleoproterozoic Ocean. *Geology* 41(6):655–658.
55. Teitler Y, et al. (2015) Ubiquitous occurrence of basaltic-derived paleosols in the Late Archean Fortescue Group, Western Australia. *Precambrian Res* 267:1–27.
56. Zhang X, Sigman DM, Morel FMM, Kraepiel AML (2014) Nitrogen isotope fractionation by alternative nitrogenases and past ocean anoxia. *Proc Natl Acad Sci U S A* 111(13):4782–4787.
57. Papineau D, et al. (2009) High primary productivity and nitrogen cycling after the Paleoproterozoic phosphogenic event in the Aravalli Supergroup, India. *Precambrian Res* 171(1–4):37–56.
58. Thomazo C, Ader M, Philippot P Extreme 15N-enrichments in 2.72-Gyr-old sediments: evidence for a turning point in the nitrogen cycle. *Geobiology* 9(2):107–120.
59. Sigman DM, Karsh KL, Casciotti KL (2009) Nitrogen Isotopes in the Ocean. *Encyclopedia of Ocean Sciences (Second Edition)*, ed Steele JH (Academic Press, Oxford), pp 40–54.
60. Rouxel O, Ludden J, Carignan J, Marin L, Fouquet Y (2002) Natural variations of Se isotopic composition determined by hydride generation multiple collector inductively coupled plasma mass spectrometry. *Geochim Cosmochim Acta* 66(18):3191–3199.
61. Olson SL, Kump LR, Kasting JF (2013) Quantifying the areal extent and dissolved oxygen concentrations of Archean oxygen oases. *Chem Geol* 362:35–43.
62. Lalonde SV, Konhauser KO (2015) Benthic perspective on Earth's oldest evidence for oxygenic photosynthesis. *Proc Natl Acad Sci* 112(4):995–1000.
63. Merchant SS, Helmann JD (2012) Elemental Economy: Microbial Strategies for Optimizing Growth in the Face of Nutrient Limitation. *Advances in Microbial Physiology, Vol 60*, ed Poole RK (Academic Press Ltd-Elsevier Science Ltd, London), pp 91–210.
64. Huertas MJ, López-Maury L, Giner-Lamia J, Sánchez-Riego AM, Florencio FJ (2014) Metals in Cyanobacteria: Analysis of the Copper, Nickel, Cobalt and Arsenic Homeostasis Mechanisms. *Life* 4(4):865–886.
65. Izon G, et al. (2015) Multiple oscillations in Neoarchaean atmospheric chemistry. *Earth Planet Sci Lett* 431:264–273.
66. Pavlov AA, Kasting JF, Eigenbrode JL, Freeman KH (2001) Organic haze in Earth's early atmosphere: Source of low-C-13 Late Archean kerogens? *Geology* 29(11):1003–1006.
67. Arney G, et al. (2016) The Pale Orange Dot: The Spectrum and Habitability of Hazy Archean Earth. *Astrobiology* 16(11):873–899.
68. Ono S, et al. (2003) New insights into Archean sulfur cycle from mass-independent sulfur isotope records from the Hamersley Basin, Australia. *Earth Planet Sci Lett* 213(1–2):15–30.
69. Scott CT, et al. (2011) Late Archean euxinic conditions before the rise of atmospheric oxygen. *Geology* 39(2):119–122.
70. Nelson DR, Trendall AF, Altermann W (1999) Chronological correlations between the Pilbara and Kaapvaal cratons. *Precambrian Res* 97(3–4):165–189.

71. Arndt N, Nelson D, Compston W, Trendall A, Thorne A (1991) The Age of the Fortescue Group, Hamersley Basin, Western-Australia, from Ion Microprobe Zircon U-Pb Results. *Aust J Earth Sci* 38(3):261–281.
72. van Kessel MAHJ, et al. (2015) Complete nitrification by a single microorganism. *Nature* 528(7583):555-559.
73. Daims H, et al. (2015) Complete nitrification by Nitrospira bacteria. *Nature* 528(7583):504-509.

Table 1: Stratigraphic stages of AIDP-2 and AIDP-3 with associated nitrogen and carbon Measurements. Strat = stratigraphic position in meters. TIC = total inorganic carbon.

Stage	Strat., m	$\delta^{15}N_{bulk}$, ‰	$\delta^{13}C_{org}$, ‰	TN, %	TOC, %	C/N*	TIC, %
AIDP-2							
III	344.18–278.75	+0.38 ± 0.61	−43.2 ± 2.5	0.08 ± 0.03	4.8 ± 2.3	81 ± 39	11.4 ± 4.4
II	377.89–344.99	+4.33 ± 0.53	−43.0 ± 1.9	0.12 ± 0.02	7.7 ± 2.4	74 ± 17	9.5 ± 2.5
I	428.16–380.37	+2.76 ± 0.71	−42.0 ± 1.5	0.04 ± 0.01	2.8 ± 0.8	95 ± 24	16.3 ± 4.9
AIDP-3							
III	127.83–66.03	+2.39 ± 0.86	−41.7 ± 1.5	0.06 ± 0.02	5.8 ± 2.4	109 ± 32	12.1 ± 8.6
II	155.75–129.65	+6.07 ± 0.36	−41.7 ± 1.0	0.06 ± 0.01	4.7 ± 0.7	85 ± 14	15.0 ± 3.0
I	204.37–156.89	+10.2 ± 2.14	−44.2 ± 0.9	0.02 ± 0.02	2.4 ± 2.1	156 ± 63	14.7 ± 2.9

Stratigraphic-stage boundaries were determined using the linear regression model described above.
*C/N ratios are given as atomic ratios.

Figures

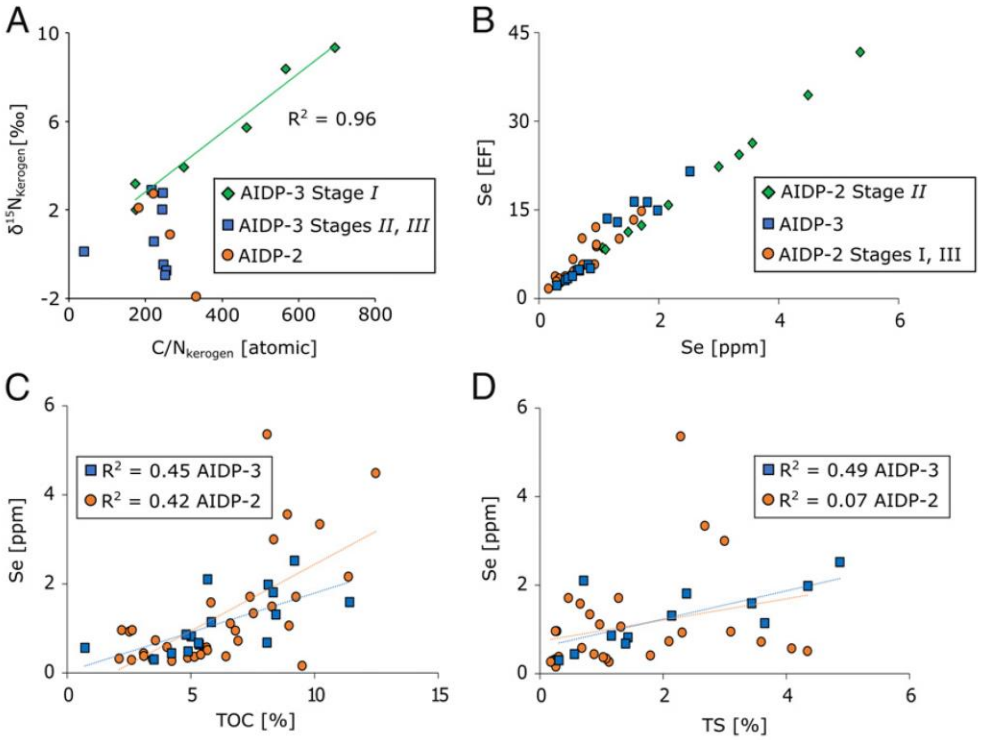

Figure 1: Crossplots of A) $\delta^{15}N_{kerogen}$ values and C/N ratios, B) Se enrichment factor [EF] and Se [ppm], C) Se [ppm] and TOC [%], and D) Se [ppm] and total sulfur [TS %]. For (A) Note the linear covariance in AIDP-3 stage *I* compared to the rest of the core. Samples from AIDP-2 come from all stages. For (B) the procedure for calculating EF is described in the SI Appendix. Note the particularly strong enrichments in AIDP-2 Stage *II*. Samples from AIDP-3 come from all stages. For (C and D) Note the weaker correlations in AIDP-2 compared to AIDP-3. The variation (and so the increase) in selenium abundance in AIDP-2 cannot be explained through variations in TOC and TS. Conversely, much of the variation in selenium abundance in AIDP-3 can be explained by variations in TOC and TS. This suggests the increase in Se during stage *II* of AIDP-2 is likely caused by an increased flux of Se to the basin.

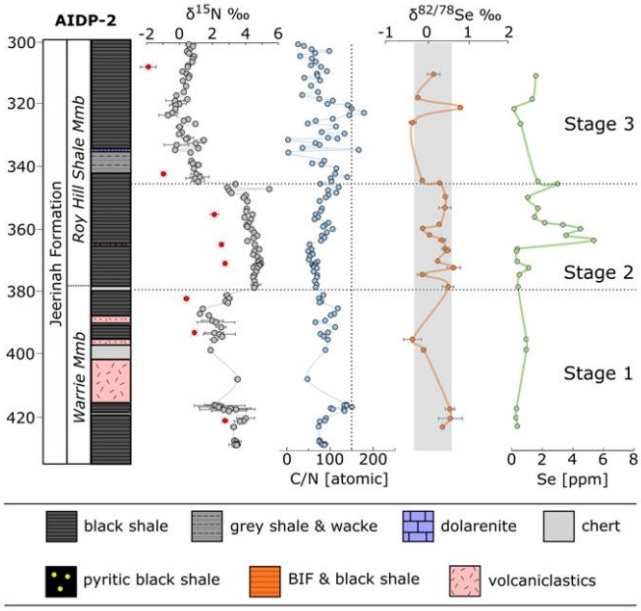

Figure 2: Chemostratigraphy of AIDP-2 showing $\delta^{15}N_{bulk}$ (grey dots), $\delta^{15}N_{kerogen}$ (red dots), C/N ratios, $\delta^{82/78}Se$, and Se concentrations. Stages are delineated by horizontal dotted lines. Shaded area for $\delta^{82/78}Se$ represents crustal values. Down-core depth is given in meters. BIF = banded iron formation.

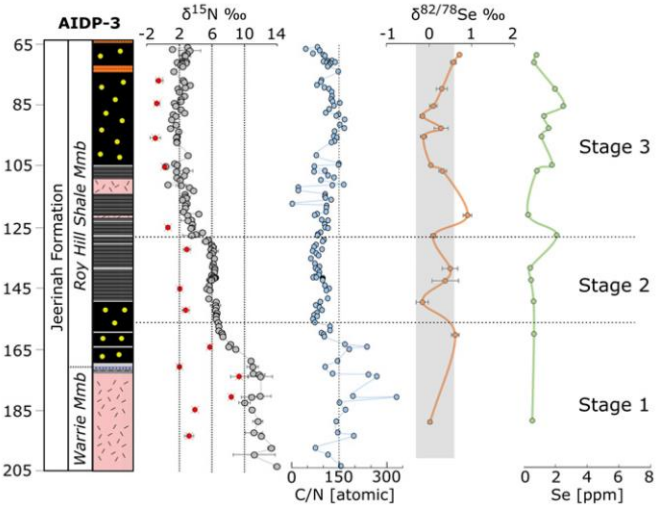

Figure 3: Chemostratigraphy of AIDP-3 showing $\delta^{15}N_{bulk}$ (grey dots), $\delta^{15}N_{kerogen}$ (red dots), C/N ratios, $\delta^{82/78}Se$, and Se concentrations. Stages are delineated by horizontal dotted lines. Lithological symbols follow the figure 2 legend. Note the different $\delta^{15}N$ and C/N scales between AIDP-2 and AIDP-3, required to accommodate Stage I of AIDP-3. Shaded area for $\delta^{82/78}Se$ represents crustal values. Down-core depth is given in meters.